6. FRACTURE MECHANICS

Applying fracture mechanics to concrete design can provide much insight on how the size of a structural element may affect the ultimate load capacity. It can also be a useful tool in predicting crack propagation. Consider a case where you are responsible for determining if a given crack in a large structure such as a concrete dam will propagate catastrophically under certain loading conditions. You can adopt a strength criterion that predicts that a crack will propagate when the stresses reach the ultimate tensile strength of the material. For sharp cracks, however, the theory of linear elasticity predicts that the stresses at the tip of the crack go to infinity, thereby assuming that the crack will propagate no matter how small the applied stress, an unlikely scenario.

Fracture mechanics, on the other hand, provides an energy criterion that does not have such drawbacks and allows for more precise predictions of the stability of the crack. The application of this energy criterion can be particularly useful when using traditional finite element methods to study cracks where mesh sensitivity becomes a problem. Figure (6.1) shows an example where the result is greatly affected by the size of the mesh when a strength criterion is used, however, little mesh sensitivity is observed when an energy criterion based on fracture mechanics is employed.

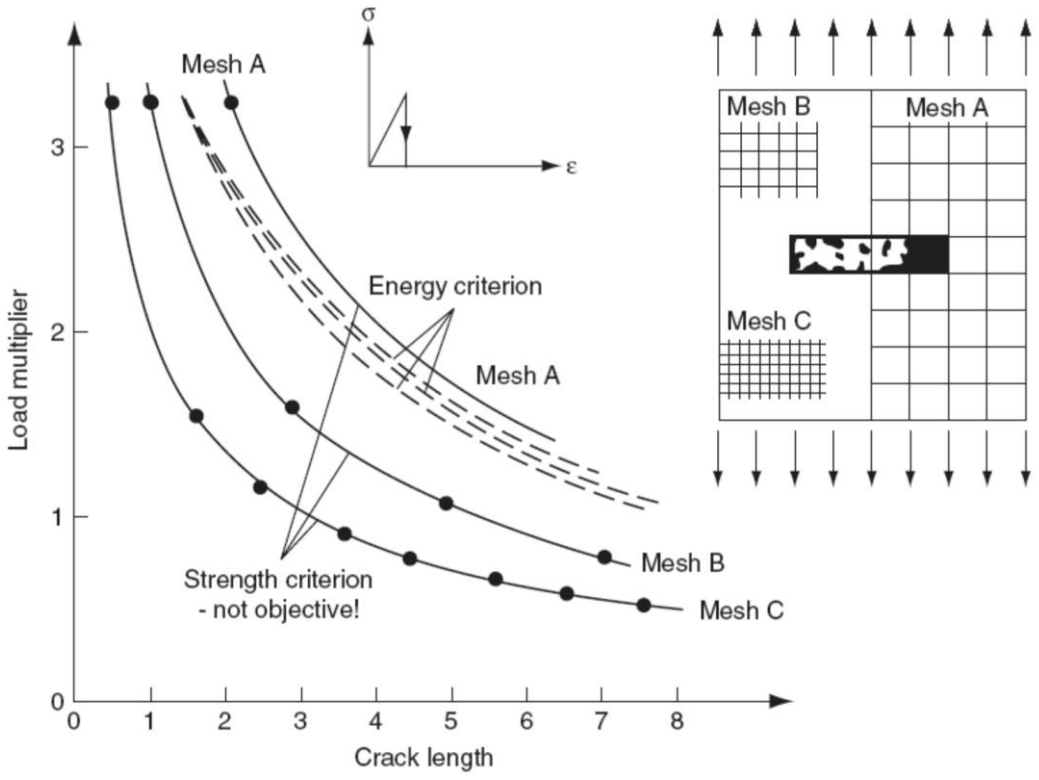

Figure (6.1): Example of mesh sensitivity.

6.1 Linear Elastic Fracture Mechanics

Figure (6.2a and b) show that when the crack is extended under constant load, the change in potential energy of the external load due to crack growth is $P\Delta x$ and the increase in strain energy is 1/2 $P\Delta x$. In other words, the decrease in potential energy of the external load is twice the increase in strain energy. During crack extension there is an increase of surface energy $4a\gamma$ (remember, the crack length is $2a$, and both the upper and lower surface of the crack should be included). Griffith (1920) used a result obtained by Inglis (1913) that the change in strain energy due to an elliptical crack in a uniformly stressed plate is $\pi a^2\sigma^2/E$, and therefore, the change in potential energy of the external load is $2\pi a^2\sigma^2/E$. The energy change of the plate, due to the introduction of the crack, is given by

$$U_{\text{cracked}} - U_{\text{uncracked}} = -\frac{2\pi a^2\sigma^2}{E} + \frac{\pi a^2\sigma^2}{E} + 4a\gamma \tag{6.1}$$

Minimizing the energy in relation to the crack length,

$$\frac{\partial}{\partial a}\left(-\frac{\pi a^2\sigma^2}{E} + 4a\gamma\right) = 0 \tag{6.2}$$

gives the critical stress (for plane stress)

$$\sigma = \sqrt{\frac{2E\gamma}{\pi a}} \tag{6.3}$$

This equation is significant because it relates the size of the imperfection ($2a$) to the tensile strength of the material. It predicts that small imperfections are less damaging than large imperfections, as observed experimentally.

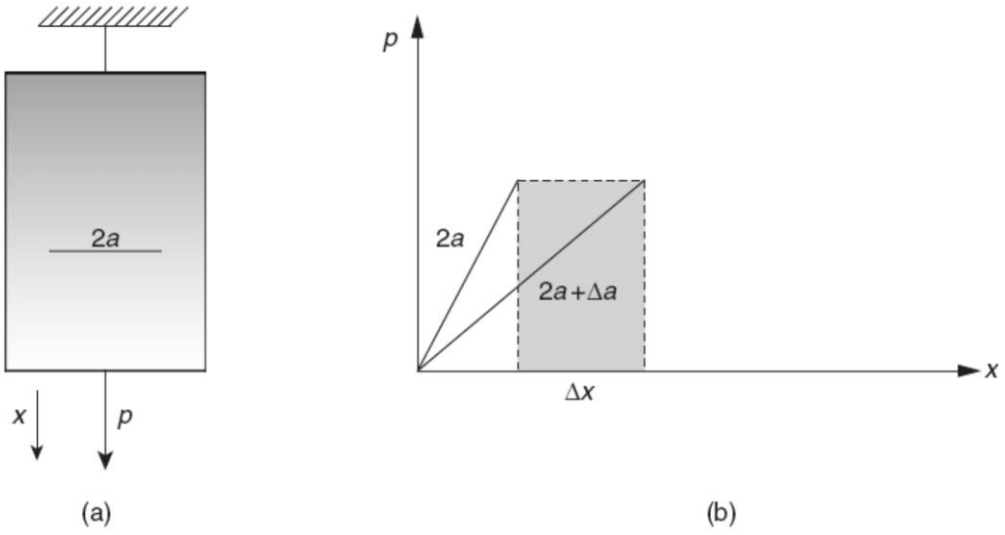

Figure (6.2): (a) Plate with crack 2*a*; (b) Load-displacement diagram.

One problem with Griffith's approach was that the surface energy obtained from his equation was found to be orders of magnitude higher than the one obtained using thermodynamical tests unrelated to fracture. The reason is that because the dissipative processes associated with the fracture propagation absorbs a significant amount of energy, the energy required for crack extension exceeds the thermodynamical value. Irwin (1957) proposed that instead of using the thermodynamic surface energy, one should measure the *characteristic surface energy* of a material in a fracture test. He introduced the quantity ***G_c as the work required to produce a unit increase in crack area***. G_c is also referred to as the *critical energy release rate*. Typically, G_c is determined experimentally, using simple specimen configuration. Once G_c for a given material is known, assuming that it is a material property, we have a powerful method for determining if a given crack will or will not propagate under any other loading condition. The process is quite simple: the energy release per unit increase crack area, G, is computed; if the energy release rate is lower than the critical energy release rate ($G < G_c$), the crack is stable. Conversely, if $G > G_c$ the crack propagates. In the particular case when the energy release is equal to the critical energy release rate ($G = G_c$) a metastable equilibrium is obtained.

The following analysis illustrates how to compute the value of Gc. Considering the plate, shown in Figure (6.2), with thickness B, we can express the energy released by crack growth Δa as

$$GB\Delta a = P\Delta x - \Delta U_e \tag{6.4}$$

Where ΔU_e is the change in elastic energy due to crack growth Δa. In the limit:

$$GB = P\frac{dx}{da} - \frac{dU_e}{da} \tag{6.5}$$

Introducing the compliance $c = \Delta x/P$, the strain energy U_e is given by

$$\Delta U_e = \frac{cP^2}{2} \tag{6.6}$$

Equation (6.5) becomes

$$GB = P\frac{d(cP)}{da} - \frac{d(cP^2/2)}{da} \tag{6.7}$$

or

$$G = \frac{P^2}{2B}\frac{dc}{da} \tag{6.8}$$

When the compliance vs. crack length has been obtained for a given specimen configuration, the critical energy release rate G_c can be determined by recording the load at fracture.

Example 4.1: Compute the energy release rate for the double cantilever beam shown in Figure (6.3). In addition, study the stability of the crack in its own plane under (**a**) load control and (**b**) displacement control. Shear deflections may be ignored.

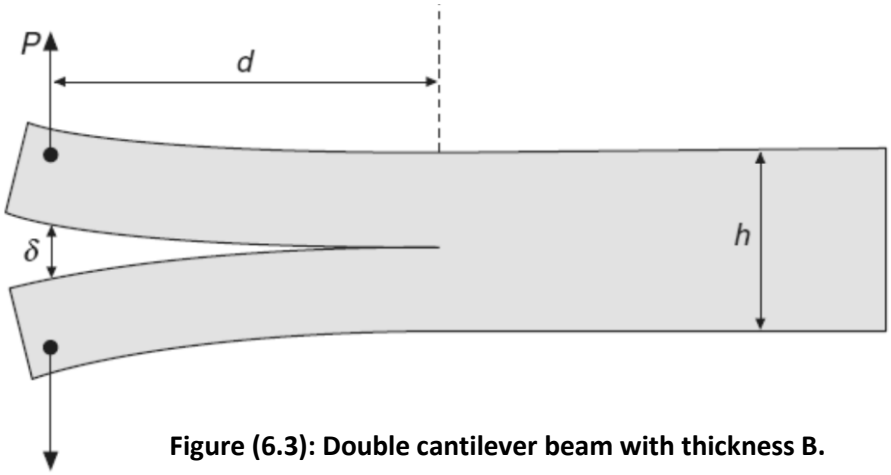

Figure (6.3): Double cantilever beam with thickness B.

The deflection of each cantilever can be easily found using simple beam theory:

$$\frac{\delta}{2} = \frac{Pa^3}{3EI} \tag{6.9}$$

where E is the elastic modulus and I is the moment of inertia,

$$I = \frac{1}{12} b \left(\frac{h}{2}\right)^3 \tag{6.10}$$

The compliance is given by

$$c = \frac{\delta}{P} = \frac{2a^3}{3EI} \tag{6.11}$$

Therefore the energy release rate is given by

$$G = \frac{P^2}{2B}\frac{dc}{da} = \frac{P^2 a^2}{BEI} \tag{6.12}$$

Stability criteria: A crack is stable if the derivative of the strain energy rate, with respect to crack length is negative. In other words,

$$\frac{1}{G}\frac{\partial G}{\partial a} < 0 \tag{6.13}$$

1. For load control:

$$\frac{\partial G}{\partial a} = \frac{2P^2 a}{BEI} \tag{6.14}$$

$(1/G)(\partial G/\partial a) = 2/a$ is a positive number, therefore the crack will propagate in an unstable way.

2. For displacement control: Combining Eqs. (6.12) and (6.11), the energy release rate can be expressed in terms of the deflection:

$$G = \frac{9EI\delta^2}{4a^4 B} \tag{6.15}$$

and

$$\frac{\partial G}{\partial a} = -\frac{9EI\delta^2}{a^5 B} \tag{6.16}$$

$(1/G)(\partial G/\partial a) = -4/a$ is a negative number, therefore, the crack will propagate in a stable manner.

6.1.1 Stress-intensity factor

Let us now analyze what happens to the stress field near the tip of a crack for the three configurations shown in Figure (6.4). The three types of relative movements of two crack surfaces are classified as (**a**) Mode I: opening or tensile mode, (**b**) Mode II: sliding or in-plane shear mode, and (**c**) Mode III: tearing or antiplane shear mode.

Most practical design situations and failures are associated with Mode I. As shown in Figure (6.5), the stresses at the tip of the crack for this mode are given by

$$\sigma_\gamma = \frac{K_I}{\sqrt{2\pi r}} \cos\frac{\varphi}{2}\left(1 + \sin\frac{\varphi}{2} + \sin\frac{3\varphi}{2}\right) \tag{6.17}$$

$$\sigma_x = \frac{K_I}{\sqrt{2\pi r}} \cos\frac{\varphi}{2}\left(1 - \sin\frac{\varphi}{2}\sin\frac{3\varphi}{2}\right) \tag{6.18}$$

$$\tau_{xy} = \frac{K_I}{\sqrt{2\pi r}}\left(\sin\frac{\varphi}{2}\cos\frac{\varphi}{2}\cos\frac{3\varphi}{2}\right) \tag{6.19}$$

K_I is called *stress-intensity factor* for Mode I. Dimensional analysis of Eqs. (6.17) to (6.19) indicates that the stress-intensity factor must be linearly related to stress and to the square root of a characteristic length. Assuming that this characteristic length is associated with the crack length, we have

$$K_I = \sigma\sqrt{a}\, f(g) \tag{6.20}$$

where $f(g)$ is a function that depends on the specimen and crack geometry.

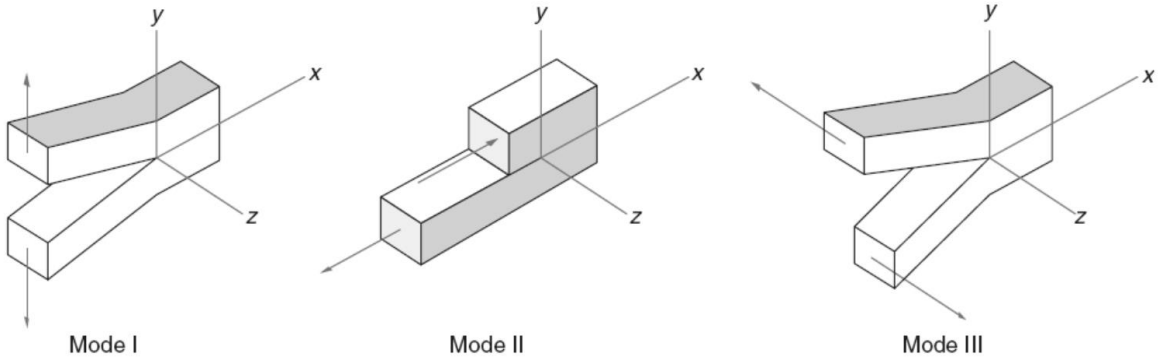

Figure (6.4): Basic modes of loading.

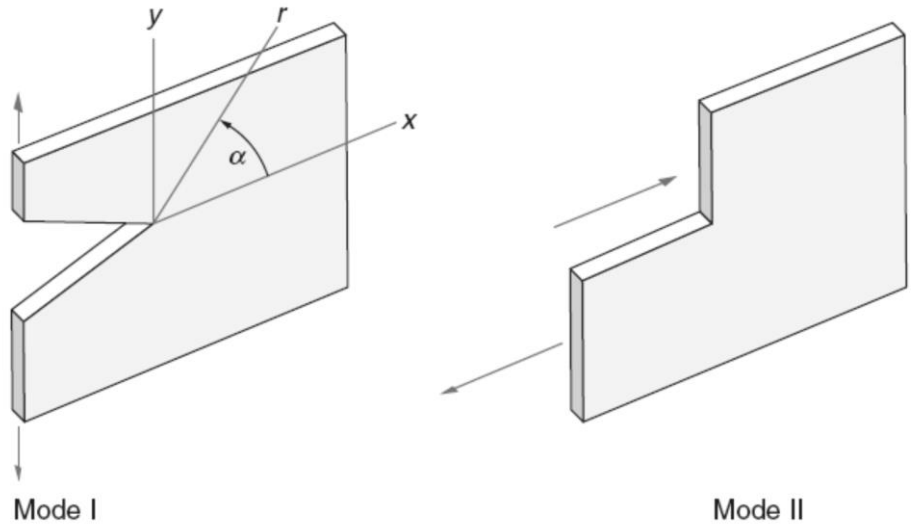

Figure (6.5): Coordinate system at the tip of the crack.

The stress-intensity factor can be computed for a variety of crack shape configurations. Suppose we measure the value of the stress at fracture in a given test. Using Eq. (6.20) we determine the critical stress intensity factor K_c or, as it is usually called in the literature, the fracture toughness. If we make the assumption that K_c is a material property (as we did for critical energy rate G_c) we have another powerful tool of predicting critical combinations of stress and crack length for other configurations of Mode I.

Irwin showed that the energy release rate and the stress intensity factor approaches are equivalent. For linear elastic behavior, considering only Mode I and plane stress condition:

$$G_I = \frac{K_I^2}{E} \tag{6.21}$$

6.2 Non-Linear Fracture Mechanics for Concrete

The first experimental research on fracture mechanics of concrete was performed by Kaplan in 1961. Subsequent research studied the effects of various parameters on K_c and G_c. Experimental studies indicated that the fracture toughness increases with increasing (**a**) aggregate volume (**b**) maximum-size aggregate, and (**c**) roughness of the aggregate. As expected, the toughness decreases with increasing water-cement ratio and increasing air content. One of the problems encountered in the early stages of this research was that, instead of being a material property, the value of the fracture toughness K_c, was strongly influenced by the size of the specimen tested. It soon became apparent that fracture mechanics measurements should not be made on small concrete specimens.

To analyze what happens to the ultimate stress when we change the dimensions of a cracked plate (Figure 6.6b) let us study the following case proposed by Cedolin (1986) The stress intensity for this configuration is given by $K = p\sqrt{\pi a} f(a/b)$ where $f(a/b)$ is a correction factor for the geometry.

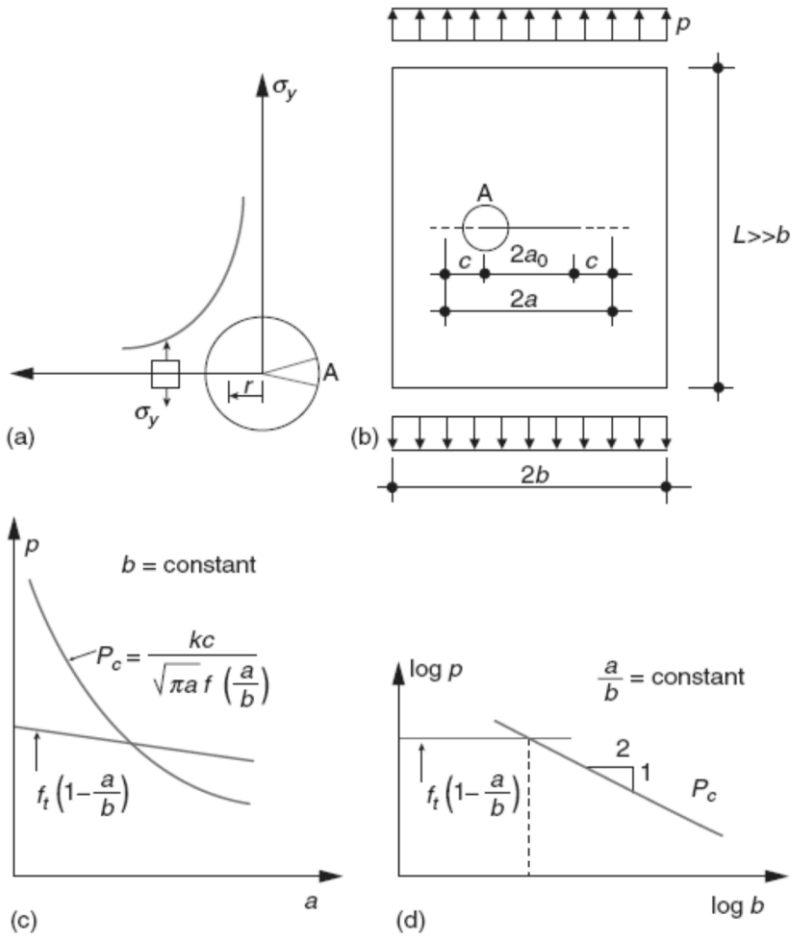

Figure (6.6): (**a**) Variation of σ_y at the crack tip in an elastic body; (**b**) cracked plate under tension; (**c**) comparison between ultimate values of applied tension, calculated according to fracture mechanics and tensile strength; (**d**) effect of plate width for geometrically similar plates.

The critical stress p_c associated with the fracture toughness K_c is given by

$$p_c = \frac{K_c}{\sqrt{\pi a} f(a/b)} \tag{6.22}$$

This relationship is shown in Figure (6.6b). Instead of the fracture mechanics criteria, let us now analyze the strength criteria. The average tensile stress f_t in the plane that contains the crack will vary because the crack dimensions affect the net section of the specimen. This relationship is given by

$$p_t 2b = f_t(2b - 2a) \tag{6.23}$$

or

$$p_t = f_t\left(1 - \frac{a}{b}\right) \tag{6.24}$$

which is also shown in Figure (6.6c). Therefore, for a small crack the strength criteria dominates, and we cannot infer fracture mechanics properties.

It is also fruitful to study the case of geometrically similar plates (a/b constant) and varying b. Equation (6.22) may be rewritten as

$$p_c = \frac{K_c}{\sqrt{b} f^*(a/b)} \tag{6.25}$$

where $f^*(a/b) = p\sqrt{\pi a/b} f(a/b)$. Since (a/b) is constant, when Eq. (6.25) is plotted as function of b in a logarithmic scale it gives a straight line with slope −1/2 (Fig. 6.6d). Equation (6.24) is also plotted in Figure (6.6d), and because a/b is constant it yields a straight line with zero slope. Again, we conclude that for small specimen sizes the strength criteria dominates and fracture mechanics properties cannot be inferred.

The ratio between the fracture mechanics criteria (Eq. 6.25) and the strength criteria (Eq. 6.24) is given by

$$\frac{p_c}{p_t} = \frac{K_c}{f_t\sqrt{b}(1-a/b) f^*(a/b)} \tag{6.26}$$

It is convenient to define a *brittleness number*, $s = K_c/f_t\sqrt{b}$, to characterize the nature of the collapse; the lower the brittleness number the more brittle the behavior of the specimen. Fracture occurs in specimens with a small brittleness number, that is, for materials with a

comparatively low fracture toughness, a high tensile strength, and in large specimens. The brittleness number characterizes the nature of the collapse for one-dimensional problems; for beams or slabs in flexure, additional information on the slenderness is necessary. It should be noted that the physical dimensions of the tensile strength $[FL^{-2}]$ and fracture toughness $[FL^{-3/2}]$ are different; however, the brittleness number is dimensionless.

Why HSC is more brittle than normal concrete

The brittleness number can also be expressed as a function of elastic modulus E and energy release rate G, instead of the fracture toughness $K_c = \sqrt{EG}/\left(f_t\sqrt{b}\right)$. This number helps to explain the experimental results where concretes made with high-strength silica fume cement paste usually have more fine microcracks than normal strength concrete (Fig. 6.6). In the high-strength matrix, the tensile strength can be two to five times greater than the normal-strength matrix; however, the increase in fracture energy or elastic modulus is not as much. Consequently, a high-strength matrix has a much lower brittleness number and is more susceptible to the development of cracks. A complete description of scaling laws for brittle materials is given by Bazant (2004).

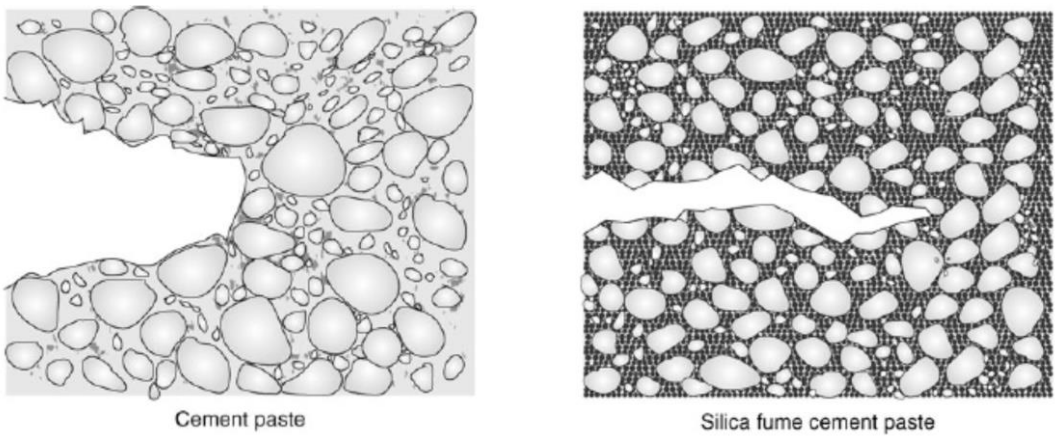

Figure (6.6): Structure of crack front in ordinary cement paste and in silica fume cement paste.

6.3 Fracture Process Zone

Microcracks in concrete originate from strain localization and develop ahead of the crack tip, creating what is referred to as a *fracture process zone*. The characterization of this zone is of fundamental importance in the development of modern nonlinear fracture mechanics for concrete. Although the experimental characterization is challenging, recently new methods have been proposed (See *Mehta* for more details).

The additional elongation in the fracture zone can be estimated by introducing the additional strains ε_w over the length of the fracture zone, as shown in Figure (6.7).

$$w = \int \varepsilon_w dx \tag{6.27}$$

Unfortunately, the real strain distribution is often very hard to incorporate into an analytical model, and to date only simplified models have been proposed. Bazant and co-workers developed the *smeared crack band model*, where the entire fracture zone is represented by a band of microcracked material with width w_c. The model assumes a linear stress-strain relationship E_c up to the tensile strength f_t and a strain-softening relationship with slope E_t. The area enclosed by the diagram in Figure (6.8) represents the fracture energy G_f given by

$$G_f = w_c \int_0^{\varepsilon_0} \sigma \, d\varepsilon_f = \frac{1}{2} w_c f_t^2 \left(\frac{1}{E_c} - \frac{1}{E_t} \right) \tag{6.28}$$

This method proved to be very successful when used with the finite element method. Further simplification is obtained when the fracture process zone is modelled as a "tied crack" (Fig. 6.7), that is, a crack with a width w and a specified stress-elongation ($\sigma - w$) relationship. Because the aim of this model is to replace the real fracture process zone by an equivalent fictitious tied crack, this representation has been called *the fictitious crack model*.

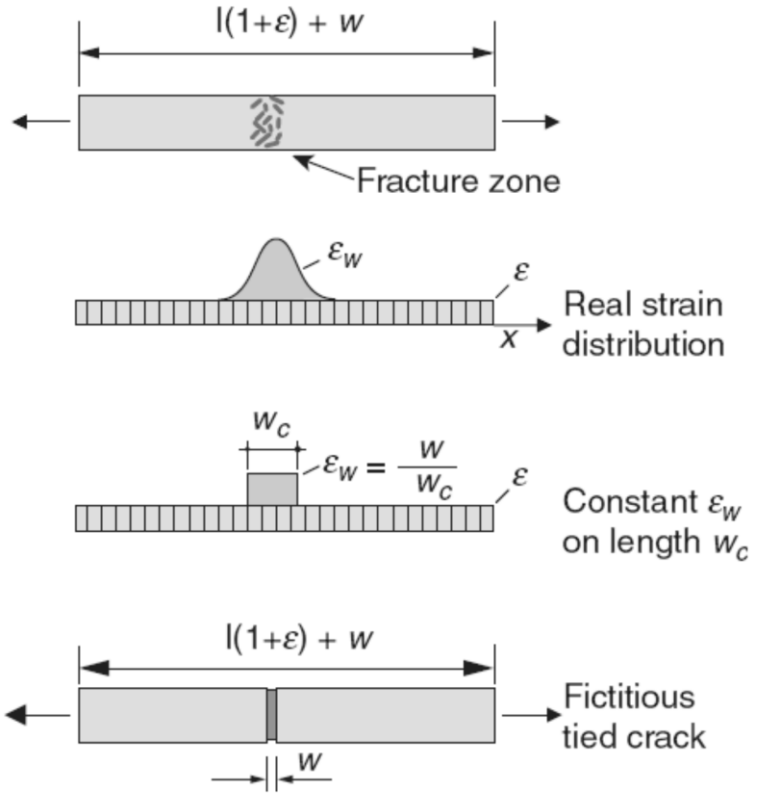

Figure (6.7): Strain distribution during fracture and two possible assumptions.

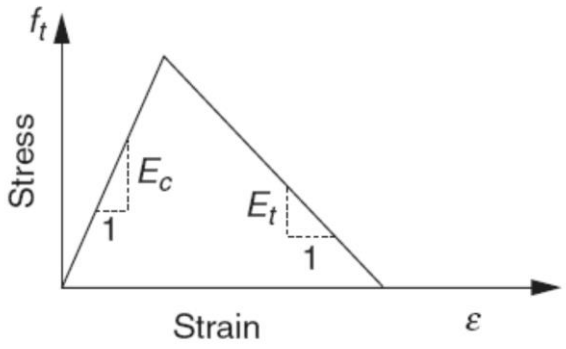

Figure (6.8): Stress-strain relationship for the smeared crack band model.

6.3.1 Fictitious crack model

The fictitious crack model was created and expanded upon by Hillerborg, Petersson, and co-workers. One of the objectives of the model is to capture the complex nature of concrete in tension. The amount of microcracking in concrete, which is in tension, is small before the peak stress is reached, therefore, the deformation ε along the specimen can be assumed to be uniform, and the total elongation Δl of the specimen can be expressed in terms of the length of the specimen l (Fig. 6.9).

$$\Delta l = l\varepsilon \tag{6.29}$$

A localized fracture zone starts to develop just after the peak load is reached. In the model, this zone is assumed to form simultaneously across an entire cross section. As the total elongation increases, the stress decreases and the region outside the fracture zone experiences an unloading, while inside the fracture zone, there is softening. The fracture zone remains localized and does not spread along the specimen, this is called strain localization, somewhat similar to that seen in plasticity. Beyond the peak stress, the total elongation of the specimen is the sum of the uniform deformation outside the fracture zone and the additional localized deformation w existing in the fracture zone, as shown in Figure (6.9b).

$$\Delta l = l\varepsilon + w \tag{6.30}$$

As illustrated in Figure (6.9c), two relationships are needed to characterize the mechanical behaviour of concrete in tension: (**1**) a stress-strain ($\sigma - \varepsilon$) relationship for the region outside the fracture zone, and (**2**) a stress-elongation ($\sigma - w$) relationship for the fracture zone. Note that in the $\sigma - \varepsilon$ diagram, the horizontal axis is given by the strain, which is nondimensional, while for the $\sigma - w$ diagram, the horizontal axis is given by the elongation, which has units of length.

Although the curves shown in Figure (6.9c) may be influenced by the rate of loading and temperature, they are assumed to be independent of the shape and size of the specimen. Figure (6.9d) shows simplified stress-strain and stress-elongation relationships. There is no fundamental reason to choose linear or bilinear relationships with the exception that they are numerically simple and seem to satisfy experimental results rather well. It should be mentioned that other researchers preferred to use a nonlinear stress-elongation ($\sigma - w$) relationship.

The fracture energy G_f is equal to the area under the stress-elongation curve.

$$G_f = \int_0^\infty \sigma(w)\, dw \tag{6.31}$$

Figure (6.10a) shows typical experimental stress-elongation curves for different concrete mixture proportions. The results presented in Figure (6.10a) are redrawn in Figure (6.10b) to show that, even with different composition, the normalized stress-elongation curves have the same shape.

For very large specimens with deep pre-existing cracks, the fracture energy G_f corresponds to the parameter G_c of the linear elastic fracture mechanics. While its measurement is fairly easy to make, the determination of the $\sigma - w$ relationship is not. Therefore, formulations, based on the fracture energy, such as the one indicated in Figure (6.9), are usually preferred in analysis.

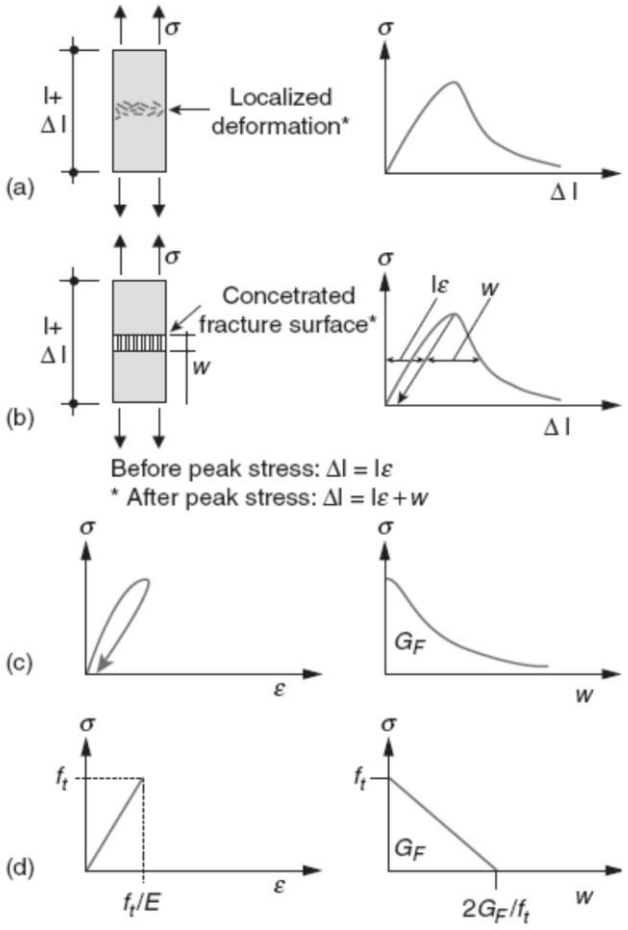

Figure (6.9): Fictitious crack model description of tensile fracture: (*a*) Realistic structural b or description of p rial.

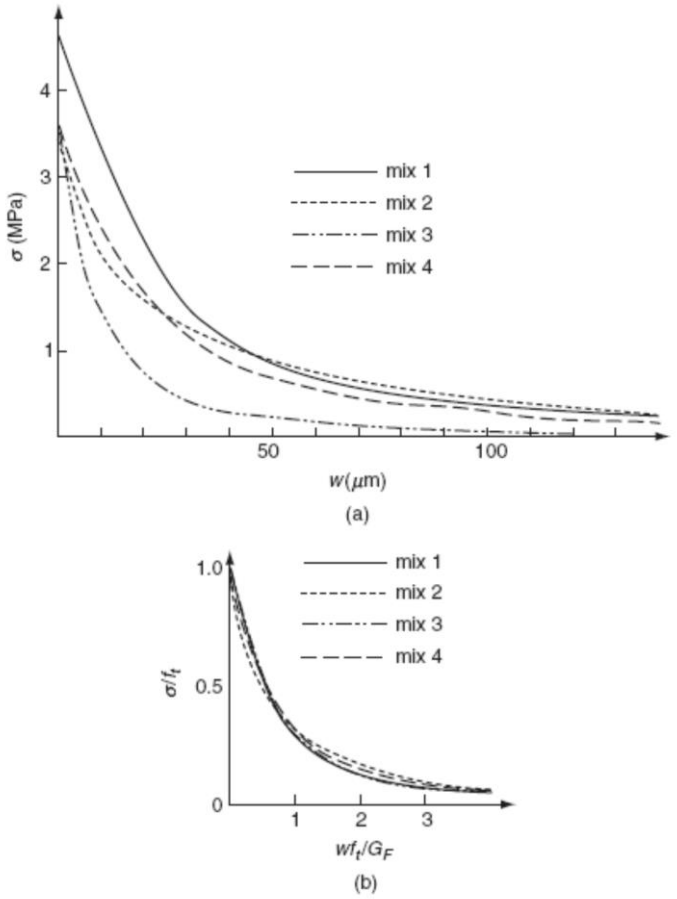

Figure (6.10): (*a*) σ-*w* curves for four concrete mixes; (*b*) the curves from (*a*) are redrawn to show that their shape is similar

The fracture energy of concrete G_f is generally determined experimentally using a notched specimen loaded in flexure, according to RILEM Recommendation TC-50 FMC. The value for G_f is obtained by computing the area under the load-deflection relationship and dividing it by the net cross-section of the specimen above the notch. When experimental data are not available, CEB-FIP model code 1990 recommends the use of the following expression:

$$G_f = \alpha_f (f_{cm}/f_{cmo})^{0.7} \tag{6.32}$$

where α_f is a coefficient, dependent on the maximum aggregate size d_{max} (Table 6.1), and f_{cmo} is equal to 10 MPa.

The stress-strain and stress-elongation curves are related in the following manner: the slope of the stress-strain diagram is E, and the slope of the stress-deformation curve is proportional to $f_t /(G_f /f_t)$. The ratio between the two slopes has units of length called the characteristic length (l_{ch}) of the material:

$$l_{ch} = \frac{EG_f}{f_t^2} \tag{6.33}$$

Table 6.1: Coefficient α_f as function of the maximum aggregate size d_{max}

$d_{\max}$ (mm)	α_f (Nmm / mm^2)
8	0.02
16	0.03
32	0.05

The characteristic length is often considered to be a material property, and it gives a measure of the brittleness of the material. Cement paste has a characteristic length in the range 5 to15 mm, mortar in the range 100 to 200 mm, and concrete 200 to 400 mm. Compared to normal-strength concrete, high-strength concretes and light-weight aggregate concrete have lower characteristic lengths.

The importance of the stress-strain and stress-elongation relationships in the design of concrete in tension must be stressed. The CEB-FIP model code 1990 recommends the following stress-strain relationships for uniaxial tension (Figure 6.11).

$$\sigma_{ct} = E_c \varepsilon_{ct} \qquad \text{for} \qquad \sigma_{ct} \leq 0.9 f_{ctm} \tag{6.34}$$

$$\sigma_{ct} = f_{ctm} - \frac{0.1 f_{ctm}}{0.00015 - (0.9 f_{ctm}/E_c)} \qquad \text{for} \qquad 0.9 f_{ctm} \leq \sigma_{ct} \leq f_{ctm} \tag{6.35}$$

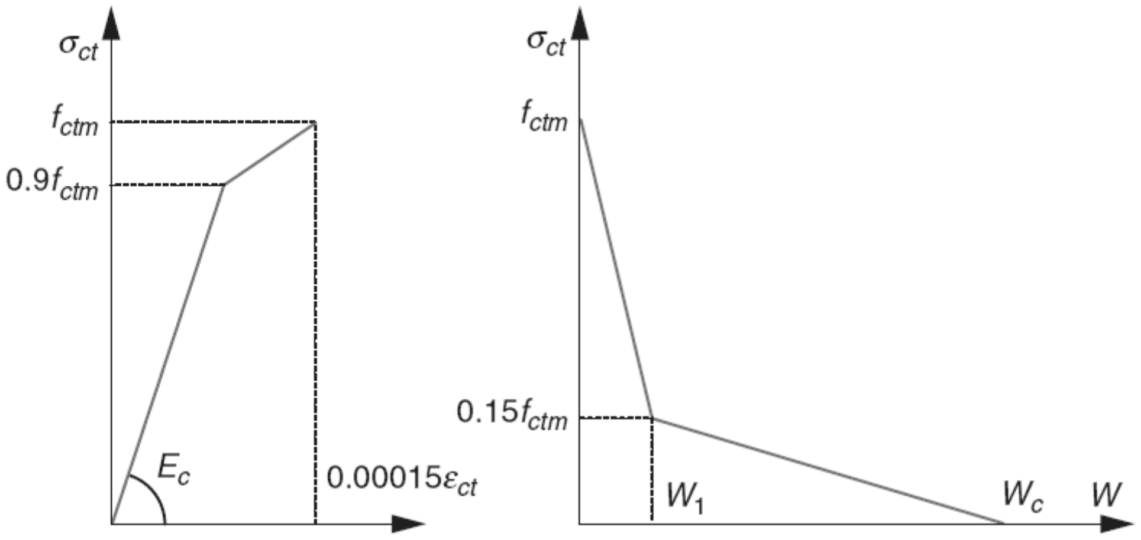

Figure (6.11): Stress-strain and stress-elongation for concrete in uniaxial tension. (From CEB-FIP Model Code 1990).

where E_c = tangent modulus of elasticity in MPa
f_{ctm} = tensile strength in MPa
σ_{ct} = tensile stress in MPa
ε_{ct} = tensile strain

For the cracked section, the following bilinear stress-crack opening relation is recommended:

$$\sigma_{ct} = f_{ctm}\left(1 - 0.85\frac{w}{w_1}\right) \quad \text{for} \quad 0.15 f_{ctm} \le \sigma_{ct} \le f_{ctm} \tag{6.36}$$

$$\sigma_{ct} = \frac{0.15 f_{ctm}}{w_c - w_1}(w_c - w) \quad \text{for} \quad 0 \le \sigma_{ct} \le 0.15\, f_{ctm} \tag{6.37}$$

and

$$w_1 = \frac{2G_f}{f_{ctm}} - 0.15\, w_c \quad \text{and} \quad w_c = \beta_F \frac{G_f}{f_{ctm}} \tag{6.38}$$

where w_1 = crack opening (mm)
w_c = crack opening (mm) for $\sigma_{ct} = 0$
G_f = fracture energy [Nm/m2]
β_F = coefficient given in Table 13-7

Table 6.1: Crack opening at $\sigma_{ct} = 0$

$d_{\max}$ (mm)	β_F
8	8
16	7
32	5